

# A Heterogeneous Graph Based Framework for Multimodal Neuroimaging Fusion Learning

Gen Shi<sup>1</sup>, Yifan Zhu<sup>1</sup>, Wenjin Liu<sup>2</sup>, and Xuesong Li<sup>1\*</sup>

<sup>1</sup>the School of Computer Science and Technology, Beijing Institute of Technology, Beijing, China

<sup>2</sup>the Department of Internal Medicine, University of Utah, SALT LAKE CITY, Utah 84132, USA

\*Corresponding author. Email: lixuesong@bit.edu.cn

November 15, 2021

## Abstract

Here, we present a Heterogeneous Graph neural network for Multimodal neuroimaging fusion learning (HGM). Traditional GNN-based models usually assume the brain network is a homogeneous graph with single type of nodes and edges. However, vast literatures have shown the heterogeneity of the human brain especially between the two hemispheres. Homogeneous brain network is insufficient to model the complicated brain state. Therefore, in this work we firstly model the brain network as heterogeneous graph with multi-type nodes (i.e., left and right hemispheric nodes) and multi-type edges (i.e., intra- and inter-hemispheric edges). Besides, we also propose a self-supervised pre-training strategy based on heterogeneous brain network to address the overfitting problem due to the complex model and small sample size. Our results on two datasets show the superiority of proposed model over other multimodal methods for disease prediction task. Besides, ablation experiments show that our model with pre-training strategy can alleviate the problem of limited training sample size.

## 1 Introduction

Neuroimaging data, such as functional Magnetic Resonance Imaging (fMRI) or Diffusion Tensor Imaging (DTI), have been widely used in disease diagnosis and study of mechanism of disease development [1–3]. DTI provides information of the structural connections (i.e., properties of white matter), while fMRI reflects the changes of the brain function and shows the abnormal properties of diseased brain. Considering that both functional and structural abnormalities may happen to the patients' brains [4–6], methods that are based on single modal data may achieve relatively worse performance in comprehensively characterizing the brain state and disease assessment. Each type of

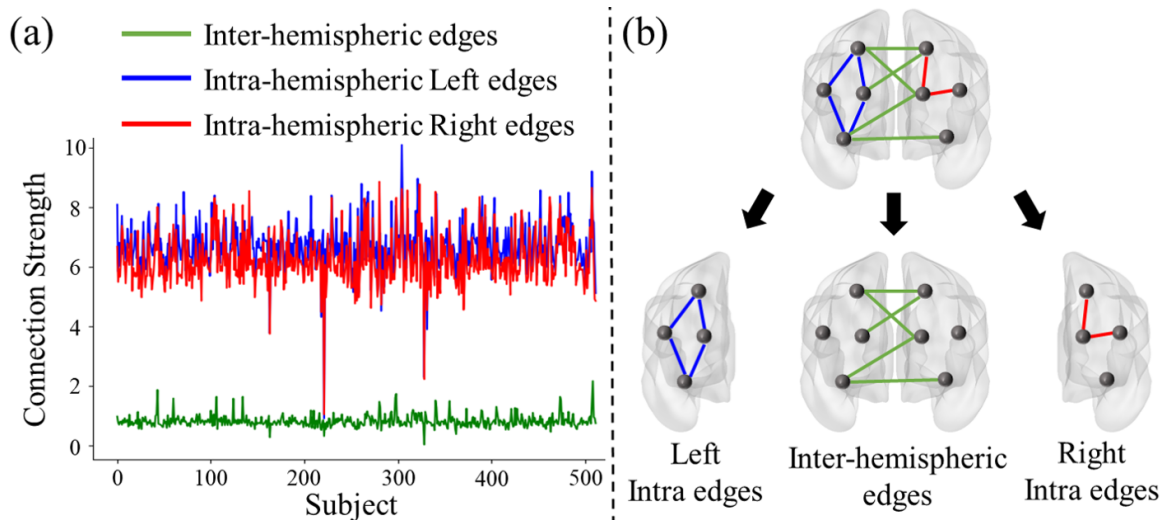


Figure 1: (a) Mean strength of intra- and inter-hemispheric edges cross subjects in ADNI dataset. (b) Division of the three type edges, including left intra-hemispheric edges (blue), inter-hemispheric edges (green), right intra-hemispheric edges (red).

neuroimaging data provides a view of brain in function or structure, and fusion of such multimodal neuroimaging plays a key role in understanding the development of disease [7, 8].

A widely used way of analysing neuroimaging data is to represent them as graph format, with brain regions as nodes and the correlations among different regions as edges. Graph-based models such Graph Neural Networks (GNNs) are proposed to integrate both graph structure and node features information [9], which has been widely used in medical image areas [10–13]. For example, Li et al. propose a multigraph-based GNN model, where graph structure is defined as Pearson correlation of BOLD signals or spatial distance between ROIs and node features are handcrafted features such as degree of connectivity, ROI centre coordinates and so on [12]. Besides, there also exist some GNN-based models for multimodal neuroimaging data fusion learning [14–16]. These methods successfully integrate multimodal neuroimaging data and show great superiority than single-modal based methods.

However, above-mentioned methods usually assume brain network is a homogeneous graph (i.e., it contains only one type nodes and edges). In fact, a large number of literatures have demonstrated the heterogeneity of two hemispheres [17–20]. The right hemisphere is shown to be dominant in responses to environment and emotion [21, 22], while the left hemisphere is dominant for languages processing [23, 24]. Therefore, the nodes in different hemispheres are considered to have different properties and nature. Besides, hemispheric specialization or brain asymmetry is a key feature of the human brain, which is also considered involving early identification of neurological diseases (e.g., Parkinson) [25, 26]. We also empirically present a statistical result from ADNI dataset to confirm our idea. We show the mean strength of three types edges (i.e., left and right intra-hemispheric edges, inter-hemispheric edges) in DTI brain network for ADNI dataset (see figure 1). It shows that left and right intra-hemispheric edges have similar strength, while they show absolutely stronger strength

than inter-hemispheric edges. This result shows that intra- and inter-hemispheric edges may have different patterns in the human brain. Based on those observations, we denote homogeneous brain network is insufficient to model the complicated brain state and activity, especially the heterogeneity of intra- and inter-interactions between the two hemispheres.

Here, we propose a Heterogeneous Graph neural Network for multimodal neuroimaging fusion learning (HGM). Inspired by the success of heterogeneous graph data mining, we firstly model the brain network as a heterogeneous graph (i.e., it contains multi-types nodes and edges). We assume left-brain nodes and right-brain nodes are different types nodes in brain network. Correspondingly, edge type between same node types (i.e., intra-hemispheric edges) and different node types (i.e., inter-hemispheric edges) is different. Our proposed model is considered capable to capture rich and complex information from the heterogeneity of the two hemispheres. Besides, we also propose a pre-training strategy designed for heterogeneous brain network based on contrastive learning method [27, 28]. This method helps us alleviate the problem of limited training data in our fine-grained and complex model. The prediction results on two datasets show that the superiority of proposed model compared with other multimodal methods.

It is worth noting that the concept of "heterogeneous graph" in this work is significantly different from that of "heterogeneous data" or "multigraph" in previous studies [70–72]. The latter is more closed to the meaning of "multimodal neuroimaging data". For instance, a multigraph usually denotes that two nodes in brain can be connected with both functional edges and structural edges (fMRI and DTI are also considered as "heterogeneous data" in this situation). If only single modal data are available, brain network in these studies can still only have single node and edge type. However, the modelling of "heterogeneous graph" in this work is inspired by the phenomenon of brain asymmetry (the nature of human brain itself), and has nothing with the data we used. The brain network can still have multi-type edges and nodes with only single modal data used in our work.

Our main contributions include the following three points: 1) We propose a new perspective to model brain network as heterogeneous graph. We theoretically and practically present the inspiration that comes from the heterogeneity between the two hemispheres and brain asymmetry. 2) We propose a novel self-supervised pre-training strategy based on heterogeneous brain network, which helps us alleviate the problem of limited training data for our model. 3) We propose a novel heterogeneous GNN model (HGM) to integrate two modal neuroimaging data (i.e., fMRI and DTI). This model can encode heterogeneous brain networks and show powerful graph representation learning with two modal data.

## 2 Related work

**Multimodal brain network learning.** The goal of multiview or multimodal fusion learning is to utilize the strength of each neuroimaging modality and builds the potential inter-modal relationships [6, 7, 15]. Unsupervised methods usually try to find a shared common node embedding across all modalities [29–32]. Such embeddings with multimodal fusion are considered to achieve better performance in downstream tasks (e.g., diseased brain classification). Besides, there is a growing

number of supervised methods especially based on GNNs [14, 33, 34]. For example, Zhang et al. propose Deep Multimodal Brain Networks (DMBN) [34]. This model tries to reconstruct FC with SC as input. Meanwhile, the node embeddings generated from GNN encoder are then readout as graph-level representations for the supervised learning tasks. It is also worth noting that there exist some literatures conduct population-level graph learning on single-modal [35, 36] and multimodal neuroimaging dataset [37]. This kind of semi-supervised learning framework is transductive and is inconvenient for application. Our proposed model HGM is an individual-level and inductive method.

As we have emphasized in Introduction part, these methods neglect the property and nature of brain itself, especially the heterogeneous feature cross two hemispheres. Our modelling method is considered to capture it.

**Heterogeneous graph representation learning.** Traditional graph embedding methods such as DeepWalk, GCN and GAT [9, 38, 39], usually assume the graph-format data contain only one type nodes and edges. This simplified method obviously losses much information since the real-world graph is usually heterogeneous information network (HIN), which consists of multi-types of nodes and edges [40, 41]. Abundant models are proposed to process the heterogeneous graph and achieve great success [42–45]. For example, Wang et al. propose Heterogeneous graph Attention Network (HAN) that utilizes two level attention mechanism (i.e., node-level and semantic-level) to capture complex structures and rich semantics in heterogeneous graph [42].

However, current heterogeneous graph based methods usually focus on node-level tasks (i.e., node classification and link prediction) and unweighted graphs. Few studies have tried to extend the application heterogeneous GNN into graph-level tasks and weighted graph (e.g., weighted brain network classification). In this work, we propose a novel heterogeneous GNN model for brain network analysis.

**Self-supervised learning based on contrastive method.** Contrastive method is an important unsupervised approach for representation learning and has been widely used in Natural Language Process [46, 47], Computer Vision areas [28, 48, 49] and Data Mining [27, 50, 51]. A score function is usually trained to classify the positive and negative pairs generated from the encoder. For example, in Deep Mutual Infomax (DMI) model [28], high-level and low-level representations from the same picture are considered positive pairs, while they are negative pairs when from different pictures.

Such self-supervised methods enable deep learning models generate high-quality representations in an unsupervised manner. In this work, we also propose a novel self-supervised pre-training method designed for heterogeneous brain networks. This method helps our model capture cross-hemispheric interactive information before the supervised signals are added, and alleviates the problem of limited training sample in medical image area.

### 3 Methods

In this section, we introduce the proposed HGM model. The overall framework of HGM can be seen in figure 2. In our proposed multimodal fusion model, DTI brain network is represented as graph structure, while FC from fMRI data is represented as node features (i.e., each row of

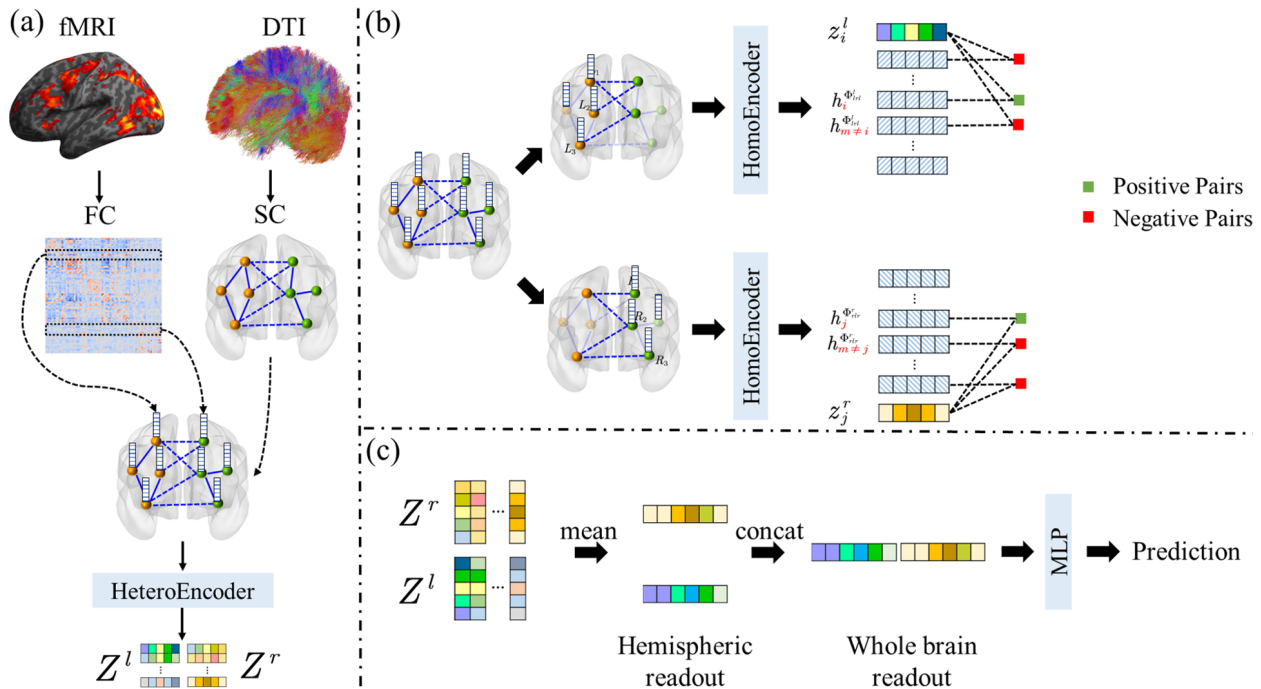


Figure 2: The overall framework of our proposed HGM model. (a) Encoder part of heterogeneous brain network. (b) Self-supervised pre-training procedure. (c) Supervised training procedure. HeteroEncoder and HomoEncoder are encoders for heterogeneous and homogeneous brain network, respectively (see section 3.2).

FC is regarded as node feature vector, see figure 2a). There are two reasons for this modeling method. Firstly, DTI data provide direct connections between brain regions, while FC reflects the correlation of BOLD signals between regions. DTI brain network may be more suitable for reflecting the structural properties of the brain. Secondly, graph structure is commonly considered sparse (e.g., social networks, molecular networks). That is to say, the number of edges is far less than the square of the number of nodes. Compared with FC, SC from DTI is more consistent with the property of sparsity.

In subsection 3.1, we introduce the several important concepts in heterogeneous brain network. We then introduce the details of HGM model in following subsections, including GNN encoder for brain network (subsection 3.2), Self-supervised pre-training strategy (subsection 3.3), Graph readout and prediction (subsection 3.4).

### 3.1 Preliminary concepts and notations

**Whole heterogeneous brain network:** A heterogeneous brain network can be defined by a four tuple  $\mathcal{G} = (\mathcal{V}, \mathcal{E}, \mathcal{T}, \mathcal{R})$ .  $\mathcal{V}$  and  $\mathcal{E}$  are node set and edge set, while  $\mathcal{T}$  and  $\mathcal{R}$  denote the sets of node types and edge types. For heterogeneous brain networks,  $|\mathcal{T}| + |\mathcal{R}| > 2$ . One example of heterogeneous brain network can be seen in figure 3. In this work, we assume that there are two node types (i.e., left and right hemispheric nodes) and two edge types (i.e., intra-hemispheric and

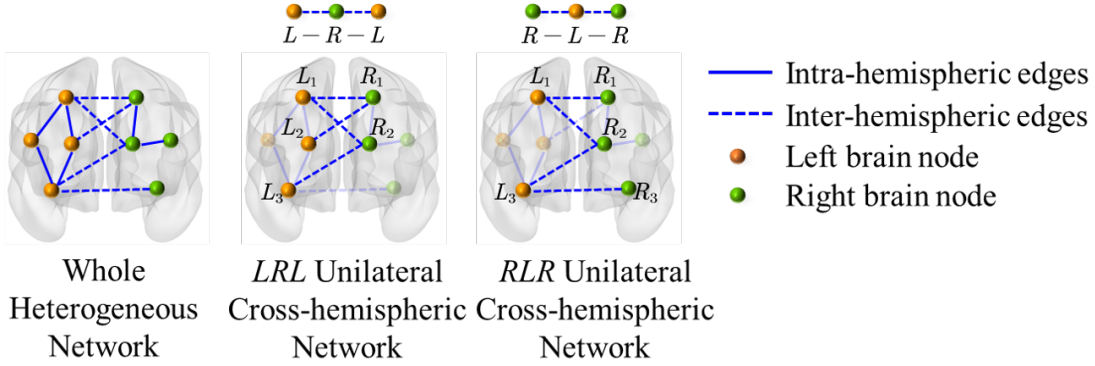


Figure 3: An Example of heterogeneous brain network (HBN) and unilateral cross-hemispheric network (UCN).

inter-hemispheric edges) in brain network.

**Cross-hemispheric path:** A cross-hemispheric path  $\Phi^m$  is defined as a symmetric path that contains only cross-hemispheric edges. The example of the two paths ( $L - R - L$  and  $R - L - R$ ) can be seen in figure 3. In fact, high-order cross-hemispheric path can also be defined in this way (e.g.,  $L - R - L - R - L$ ). We consider that cross-hemispheric paths in brain network denote the cross-hemisphere message interaction. Considering that the hemispheric lateralization or brain asymmetry is a fundamental fact for the human brain, we assume the such paths may contain valuable information. Besides, cross-hemispheric path can be regarded as a special form of meta-path in HIN.

**Unilateral cross-hemispheric network.** Cross-hemispheric path represents indirect neighboring relationship, which is different from the direction connection in the view of whole brain network. For example, in figure 3,  $L_2$  and  $L_3$  are the neighbors of  $L_1$  through  $L_1 - R_1 - L_2$  and  $L_1 - R_2 - L_3$ . This kind of connections denotes different neural process, compared with direct connections  $L_1 - L_2$ . Besides, latent neighbouring relationship can be uncovered. For example,  $R_3$  are regarded as the neighbor of  $R_2$  via  $R_3 - L_3 - R_2$ , though there is no direct connection between them. For a path  $\Phi^m$ , neighbors set  $\mathcal{N}^{\Phi^m}$  for each node type  $m$  can be obtained through such neighboring relationship. Then we can construct an unilateral cross-hemispheric brain network  $\mathcal{G}^{\Phi^m}$  based on  $\mathcal{N}^{\Phi^m}$ .

We highlight the difference of whole heterogeneous brain network (WHN) and unilateral cross-hemispheric network (UCN) here. WHN is a heterogeneous graph while UCN is a homogeneous graph that contains only single-hemispheric nodes. WHN represents the 1rd direct connections for the whole brain while UCN represents the 2rd cross-hemispheric connections for single hemisphere.

### 3.2 GNN encoder for brain networks

**Encoder for whole heterogeneous brain network.** The WHN in this work contains two node and edge types. Traditional homogeneous GNN model cannot directly encode WHN infor-

mation. We consider each node aggregates messages from two edge patterns (intra- and inter-hemispheric edges) respectively, and finally generates the node representation. Besides, for each edge type, the edge feature (e.g., connection strength) should be also taken into consideration.

Specifically, considering neighbors set  $\mathcal{N}_i^r$  that denotes the set of neighbors connected to node  $i$  with edge type  $r$  (e.g.,  $\mathcal{N}_i^r$  can be  $\mathcal{N}_i^{L-L}$  or  $\mathcal{N}_i^{L-R}$  for left brain nodes), node  $i$  receives the message sent from neighbors through edge type-related projection matrix  $W_r$ . Node  $i$  updates its representations via aggregating the messages from all edge types. This encoder can be expressed as:

$$h_i^{(l)} = \sigma \left( \frac{1}{C(i)} \left( \sum_{r \in \mathcal{R}_i} \sum_{j \in \mathcal{N}_i^r} \frac{1}{|\mathcal{N}_i^r|} W_r^{(l-1)} f_r^{(l-1)}(e_{ij}) \otimes h_j^{(l-1)} + W_o^{(l-1)} h_i^{(l-1)} \right) \right) \quad (1)$$

where  $h_i^{(l)}$  is node hidden representation after graph convolution in layer  $l$  and  $C(i)$  is normalization coefficient. We set  $C(i) = |\mathcal{R}_i| + 1$ .  $\mathcal{R}_i$  is the set of edge types connected to node  $i$ .  $\sigma(\cdot)$  is non-linear activation function such as ReLU.  $W_r^{(l)}$ ,  $W_o^{(l)}$  are the trainable parameters in layer  $l$ .

In this encoder, edge feature  $e_{ij}$  is also take into consideration.  $f_r^{(l)}(\cdot)$  is a function that maps  $e_{ij}$  into the same space with  $h_j^{(l)}$  and  $\otimes$  is the Hadamard product. In this work, there are only two edge types for each node (i.e.,  $|\mathcal{R}_i| = 2$ ). Edge weight in SC is modelled as  $e_{ij}$  and one linear layer is trained as mapping function  $f_r^{(l)}(\cdot)$ .

**Encoder for Unilateral cross-hemispheric network.** UCN is a simple homogeneous graph. More importantly, we model the UCN as unweighted graph. There are three reasons why we don't take the edge feature into consideration for UCN. Firstly, it is hard to determine the connection strength for indirect edges (two-hop edges). More detailed modelling method may complicate the model and increase the risk of overfitting. Secondly, figure 1a shows that the strength of inter-hemispheric edges is small. The information that inter-hemispheric edges exist or not may be more important than the information of its connection strength. Thirdly, the strength of inter-hemispheric edges has been taken into consideration in WHN encoder part, therefore no information is lost here.

Based on above-mentioned reasons, UCN is considered as homogeneous and unweighted graph in work, and we adopt a traditional GNN model (GCN) [9] with self loop as the encoder, which can be expressed as:

$$h_i^{\Phi^m} = \sigma \left( \sum_{j \in \mathcal{N}_i^{\Phi^m}} \frac{1}{\sqrt{(d_i + 1)(d_j + 1)}} W_{\Phi^m} h_j \right) \quad (2)$$

where  $d_i$  is the degree of node  $i$  in  $\mathcal{G}^{\Phi^m}$  and  $W_{\Phi^m}$  is the trainable parameter for cross-hemispheric path  $\Phi^m$ .

### 3.3 Self-supervised pre-training strategy

In this pre-training procedure, our goal is to maximize the mutual information (MI) between  $h_i^{(L)}$  and  $h_i^{\Phi^m}$  for each node  $i$  ( $L$  is the Last layer of heterogeneous GNN encoder). This optimization procedure helps  $h_i^{(L)}$  capture more information from  $h_i^{\Phi^m}$ , and has following benefits:

- 1) Enlarge the receptive field of graph convolution with shallow model. WHN represents only the

1rd connection relationship, while UCN represents 2rd cross-hemispheric dependence relationship. Maximization of the MI helps the heterogeneous GNN encoder generate powerful  $h_i^{(L)}$  with less graph convolutional layers and decrease the risk of overfitting.

2) Help heterogeneous GNN encoder capture cross-hemispheric semantics. UCN characterizes the cross-hemispheric neural process which is different from direct connections in single hemisphere. The optimization procedure provides a opportunity for heterogeneous GNN encoder to capture the features of such cross-hemispheric interactive messages.

3) Denoising and dimension reduction before supervised signals added. The optimization procedure reduces the dimension of node embeddings without supervised signals, which provides a good starting point for the optimization process of supervised learning. It also helps alleviate the problem of limited training sample for medical image analysis.

We now introduce how to estimate the MI between  $h_i^{(L)}$  and  $h_i^{\Phi^m}$ . The whole optimization procedure can be expressed as:

$$\hat{W}_{\mathcal{R}}, \hat{W}_{\Phi} = \max_{W_{\mathcal{R}}, W_{\Phi}} MI(h^{(L)}, h^{\Phi}) \quad (3)$$

where  $W_{\mathcal{R}}, W_{\Phi}$  are parameters for WHN encoder and UCN encoder, respectively. Based on [28, 52, 53], MI can be estimated as:

$$\begin{aligned} MI(h^{(L)}, h^{\Phi^m}) &\propto \max_{D(\cdot)} \\ &\left( \mathbb{E}_{(h^{(L)}, h^{\Phi^m}) \sim p(h^{(L)})p(h^{\Phi^m})} \log(1 - \mathcal{D}(h^{(L)}, h^{\Phi^m})) \right. \\ &\left. + \mathbb{E}_{(h^{(L)}, h^{\Phi^m}) \sim p(h^{(L)}, h^{\Phi^m})} \log(\mathcal{D}(h^{(L)}, h^{\Phi^m})) \right) \end{aligned} \quad (4)$$

where  $p(h^{(L)}, h^{\Phi^m})$  is the joint distribution for  $h^{(L)}$  and  $h^{\Phi^m}$ , while  $p(h^{(L)})p(h^{\Phi^m})$  is the product of their marginal distribution. The key is how to understand  $p(h^{(L)}, h^{\Phi^m})$  and  $p(h^{(L)})p(h^{\Phi^m})$ .

Inspired by previous studies [27, 73],  $\mathbb{E}_{(h^{(L)}, h^{\Phi^m}) \sim p(h^{(L)}, h^{\Phi^m})}$  is regarded as sampling  $(h^{(L)}, h^{\Phi^m})$  from same node (i.e., positive pair), while  $\mathbb{E}_{(h^{(L)}, h^{\Phi^m}) \sim p(h^{(L)})p(h^{\Phi^m})}$  is sampling  $(h^{(L)}, h^{\Phi^m})$  from different nodes (i.e., negative pair). Discriminator function  $\mathcal{D}(\cdot)$  is trained to distinguish positive pairs and negative pairs. Therefore, for a specific node type  $m$ , the final optimization objective can be expressed as:

$$\mathcal{L}_m(h^{(L)}, h^{\Phi^m}) = \frac{1}{C(m)} \sum_{i \in \mathcal{N}^{(m)}} \sum_{\Phi_p^m \in \Phi^m} \left( K \cdot \log \mathcal{D}(h_i^{(L)}, h_i^{\Phi_p^m}) + \sum_{j \neq i}^K \log(1 - \mathcal{D}(h_i^{(L)}, h_j^{\Phi_p^m})) \right) \quad (5)$$

where  $C(m)$  is the normalized coefficient. We set  $C(m) = |\mathcal{N}^{(m)}| \cdot |\Phi^m|$  in this work.  $K$  is the number of negative sampling. Larger value of  $K$  will increase the difficulty of contrastive learning procedure.

Considering that there are only two node types (i.e.,  $m \in \{LN, RN\}$ ) and each node has only



single cross-hemispheric path (i.e.,  $|\Phi^m| = 1$ ), the whole optimization objective can be simplified as:

$$\mathcal{L} = \frac{1}{2} \sum_{m \in \{LN, RN\}} \frac{1}{|\mathcal{N}^{(m)}|} \sum_{i \in \mathcal{N}^{(m)}} \left( K \cdot \log \mathcal{D} \left( h_i^{(L)}, h_i^{\Phi^m} \right) + \sum_{j \neq i}^K \log \left( 1 - \mathcal{D} \left( h_i^{(L)}, h_j^{\Phi^m} \right) \right) \right) \quad (6)$$

In this work, we use bilinear layer [27] with trainable parameter  $W_D$  as discriminator function:

$$\mathcal{D} \left( h_i^{(L)}, h_i^{\Phi^m} \right) = \sigma \left( \left( h_i^{(L)} \right)^T W_D h_i^{\Phi^m} \right) \quad (7)$$

### 3.4 Brain network readout and disease prediction

After pre-training procedure, the output of heterogeneous GNN encoder  $h^{(L)}$  is used for graph-level readout and supervised learning. Compared with  $h^{\Phi^m}$ ,  $h^{(L)}$  is considered to capture more global properties of the human brain. Therefore, it may be more suitable for brain network classification task.

For each subject  $t$ , it has a set of node representations  $H_t = \left( h_1^{(L)}, h_2^{(L)}, \dots, h_N^{(L)} \right)_{N \times d}$  ( $N$  is the number of ROIs in atlas,  $d$  is the hidden dimension) after pre-training. We simply average  $H_t$  cross feature dimensions to obtain the graph-level representation:

$$gh_t = \text{Mean}(H_t, 1) \quad (8)$$

where  $gh_t$  is the graph-level representation with shape  $(1, N)$ . Then a MLP is trained to get the prediction for subject  $t$ , and Cross Entropy is used to estimate the loss. This supervised procedure can be expressed as:

$$\hat{y}_t = \text{MLP}(gh_t) \quad (9)$$

$$\mathcal{L}_s = -\frac{1}{T} \sum_T [y_t \cdot \log(\hat{y}_t) + (1 - y_t) \cdot \log(1 - \hat{y}_t)] \quad (10)$$

## 4 Datasets and preprocessing

### 4.1 Datasets

**OH (Orthostatic Hypotension):** This dataset contains 224 subjects, 147 of which are patients with OH and the rest are Health Control. fMRI imaging data are acquired using a 3T GE scanner (Signa HDxt, GE Healthcare) with an 8-channel head coil. Resting-state data are acquired using a gradient-echo planar imaging (EPI) sequence. For the resting-state fMRI scanning, the following parameters are used: TR = 2000 ms; TE = 30 ms; field of view (FOV) =  $240 \times 240$  mm<sup>2</sup>; acquisition matrix =  $64 \times 64$ ; FA = 90°; slice thickness = 4.4 mm and 32 transverse slices. The resting state scan lasts 8 min and 20s (250 vol). DTI data are collected using an echo planar imaging (EPI) sequence with the following parameters: b-value = 1000 s/mm<sup>2</sup>, flip angle = 90°, TR = 13500 ms, TE = 87.4 ms, FOV =  $240 \times 240$  mm<sup>2</sup>, acquisition matrix =  $240 \times 240$ , 50 contiguous

slices, resulting in a voxel dimension of  $1 \times 1 \times 3 \text{ mm}^3$ . A total of 20 independent and non-collinear diffusion encoding directions, and one additional image with no diffusion weighting ( $b = 0$ ) are acquired. High resolution T1-weighted structural images in the coronal view are acquired with a slice thickness of 1mm without a gap, flip angle =  $15^\circ$ , TR = 6.1 ms, TE = 3.2 ms, FOV =  $240 \times 240 \text{ mm}^2$  (matrix =  $240 \times 240 \times 146$ ).

Since OH dataset is imbalanced, we adopt a data augmentation strategy in [12] to balance the dataset. For each ROI in one subject, the mean time signal is extracted from a random 1/3 of voxels instead of the whole voxels. We augment the patient subjects 10 times and the HC subjects 20 times, resulting in totally 1470 brain network with OH disease and 1540 HC brain networks, separately.

**ADNI:** All image data are downloaded from ADNI is in DICOM format originally. More detailed information of the parameters can be found from the ADNI website. This dataset contains 512 subjects, consisting of 250 Cognitive Normal (CN), 85 Mild Cognitive Impairment (MCI), 84 Early MCI (EMCI), 58 Alzheimer’s Disease (AD), 35 Late MCI (LMCI). For the sake of simplicity, MCI, ECMI, LMCI and AD are regarded as patients in this work, and a binary classification task is conducted in this dataset.

## 4.2 Preprocessing

For fMRI data, GREYNA software is used [54]. The procedure contains removing first several volumes of images to ensure magnetization equilibrium, slice timing correction with the first slice, head-motion estimation and correction with a 0.01-0.10 Hz frequency bandpass, the first scan of fMRI time series co-registered to the T1-weighted images, which is then normalized to the Montreal Neurological Institute (MNI) template space and spatially smoothing with a Gaussian kernel. For node definition of brain network, Brainnetome Atlas (246 ROIs) [55] are used in the two datasets. The mean time series of each ROI is obtained by averaging the BOLD time series over the voxels. The edges of fMRI brain networks are computed by z-transformation values of Pearson correlation coefficients.

For DTI data, deterministic tractography method is performed by using DSI studio toolbox (<http://dsi-studio.labsolver.org>). A deterministic fiber tracking algorithm [56] is used for fiber-tracking after the diffusion tensor is calculated. The angular threshold is 70 degrees and step size is 1 mm. Tracks with the length shorter than 20 mm or longer than 180 mm are discarded. The number of connected fibers to each of the rest of the regions is calculated separately, which is defined as the edge weight between regions in DTI brain network.

# 5 Results

## 5.1 Baselines and implementation details

GCN [9] and GAT [39] are originally designed for node classification task in social networks. GCN simplifies the spectral domain graph convolution and conducts the spatial graph convolution via 1-hop neighbors. GAT adopts self-attention mechanism to determine the importance of the node neighbors and show better performance than GCN model. CoRegSC [30] and M-GEHB [31]

Table 1: Disease prediction performance compared with State-of-The-Art methods

Dataset	OH			ADNI		
Method	Accuracy	F1	AUC	Accuracy	F1	AUC
GCN	63.80±05.79	61.88±05.90	62.70±07.49	71.88±03.45	71.78±03.18	71.92±03.47
GAT	64.00±02.51	64.26±02.34	63.15±02.97	71.88±02.47	72.63±02.37	71.85±02.49
CoRegSC	59.77±09.19	68.26±07.23	56.92±10.34	64.06±02.68	62.67±03.58	64.19±02.65
GEHB	53.13±05.38	63.37±04.30	49.23±07.10	51.57±02.83	51.01±02.42	51.62±02.85
ABD	65.86±06.47	66.96±06.56	65.50±06.58	72.07±03.54	73.03±04.24	72.00±03.51
MGCN	68.36±04.17	71.03±02.02	68.35±04.25	70.69±02.33	70.91±03.43	70.71±02.28
DMBN	64.77±03.01	66.02±02.80	63.57±03.66	61.72±02.44	64.87±02.86	61.51±02.66
HGM	<b>73.55±06.68</b>	<b>75.50±04.75</b>	<b>73.82±06.25</b>	<b>73.04±01.06</b>	<b>73.46±02.01</b>	<b>75.85±02.65</b>

are two unsupervised methods. CoRegSC proposed the centroid-based Co-regularization algorithm, which generates central embeddings for multi-view data. M-GEHB considers hub detection in multi view graph dimensionality reduction research, The experimental results show that the hub node detection mechanism can make the two tasks interact and promote each other. ABD [33], MGCN and DMBN [34] are homogeneous GNN-based methods designed for multimodal neuroimaging fusion learning. ABD adopts attention mechanism to generate representations from 1-and 2-hop brain network. MGCN pioneers conducting graph convolution in row and column separately for brain network. DMBN propose a new loss function to reconstruct FC through node hidden representations generated from SC.

We report three metrics (classification accuracy, F1 score, and AUC) for performance evaluation. The mean value of 5-fold cross-validation is reported. Our source code is available at website<sup>1</sup>. Implementation details for each method can be seen in supplementary materiel section A.1.

## 5.2 Disease prediction

We first compare our method with prior state-of-the-art multimodal methods in the two datasets. The results are shown in table 1.

(Please note that, as the ADNI dataset comes from multi center sites, the image data are highly heterogeneous cross the subjects. Considering the fact that sample size in this work is relatively large (512 subjects), the comparison of the disease prediction performance directly with the existing works is meaningless.)

The results show that our proposed model achieves best performance among all methods. For OH dataset, the proposed model achieved state-of-the-art performance (73.55% accuracy, 75.50% F1 score and 73.82 AUC), around 5% higher than the best existing methods. For ADNI dataset, the proposed model also obtains the best prediction scores, with 73.04% accuracy, 73.46% F1 scores and 75.85 AUC, respectively. Compared with those models for homogeneous brain network, proposed model utilizes heterogeneous information in brain network and achieves best performance.

<sup>1</sup><https://github.com/shigen97/HGM>

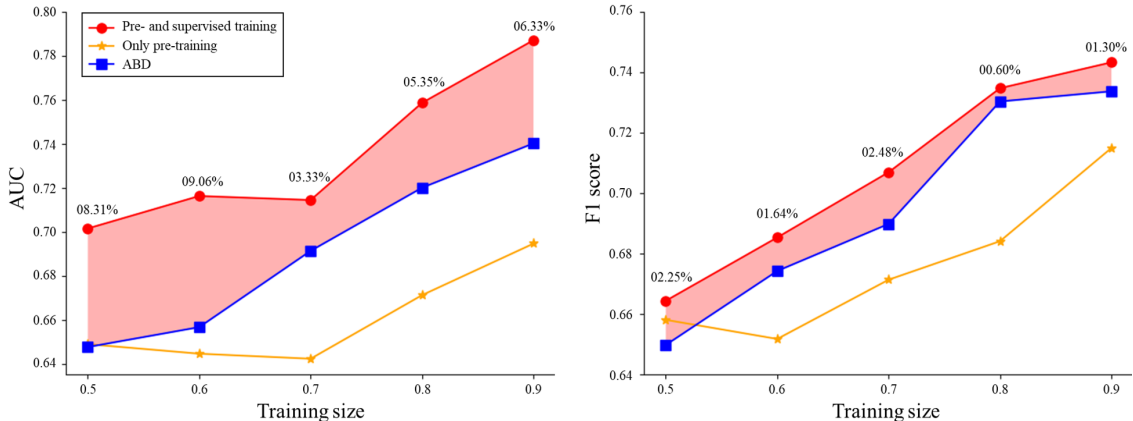


Figure 4: The effect of pre-training strategy varies with training size. The percentage number represents the relative improvement rate of our proposed model compared with ABD (i.e.,  $(Metric_{HGM} - Metric_{ABD})/Metric_{ABD}$ ,  $Metric$  is AUC or F1 score).

Table 2: Influence of the pre-training strategy on the prediction performance in the two datasets. HGM (w/o) denotes the model without pre-training procedure and HGM (only) denotes the unsupervised model that only contains the pre-training procedure (i.e., without supervised finetune procedure).

Datasets	OH			ADNI		
	Accuracy	F1-score	AUC	Accuracy	F1-score	AUC
HGM (w/o)	70.28±05.12	70.92±06.22	70.11±05.41	68.15±03.75	67.41±05.21	72.62±03.09
HGM (only)	69.45±02.11	71.16±02.20	69.19±01.75	67.18±03.21	68.41±02.96	67.13±03.23
HGM (both)	73.55±06.68	75.50±04.75	73.82±06.25	73.04±01.06	73.46±02.01	75.85±02.65

### 5.3 Analysis of the pre-training strategy

In this subsection, we investigate the influence of proposed self-supervised pre-training strategy on our model. We show the results without pre-training and only with pre-training in table 2. The metrics decrease around 4% for the two datasets in terms of accuracy, F1 score and AUC. The results demonstrate the importance of pre-training for our complex model.

In addition, the heterogeneity of image data may highly influence the performance of self-supervised learning. The results in table 2 show that self-supervised learning performs well in OH dataset while poorly in ADNI dataset. In fact, self-supervised learning tries to learn inner-data relationships. Therefore, image data collected from multi center sites may be highly heterogeneous and cannot ensure the model a good performance in a self-supervised manner. This may also be the possible reason why DMBN achieves a relatively worse performance in ADNI dataset. DMBN tries to reconstruct the FC with the SC as input, and the different patterns generated from the data heterogeneity may harm the performance.

Besides, we investigate the influence of training set size. We take the public dataset ADNI as an example (also in following subsections). We randomly select training set with a rate  $r$  ( $0.5 \sim 0.9$ ) and conduct the same experiment for our model and ABD that performs the best in baselines. We repeat the experiment 5 times and report the mean AUC and F1 score. The results are shown in

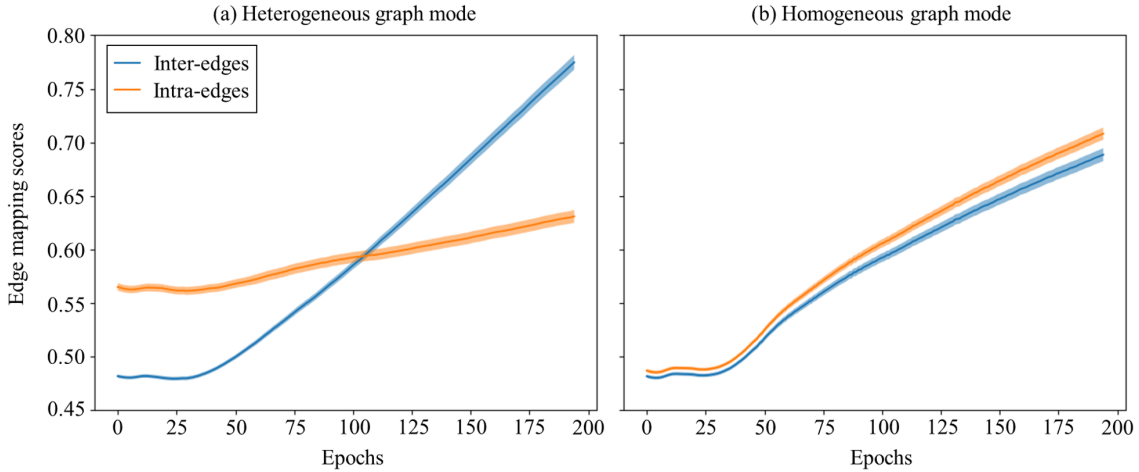


Figure 5: The change of Edge Mapping Scores for two type edges during training epochs.

Table 3: Influence of the hemispheric heterogeneity for our model. HGM (homo mode) denotes our model without heterogeneous graph setting. HGM (intra-edges) and HGM (inter-edges) denotes that the graph structure contains only inter- and intra- hemispheric edges.

Methods	Accuracy	F1-score	AUC
HGM (homo mode)	68.55±03.19	67.45±04.32	70.03±04.21
HGM (intra-edges)	65.03±03.62	63.67±03.79	68.54±03.64
HGM (inter-edges)	67.39±03.07	66.37±03.32	70.58±04.62
HGM	73.04±01.06	73.46±02.01	75.85±02.65

figure 3.

With the decrease of training set samples, the performances of all the models decline, while the difference between our model and ABD gradually increases. We also show the relative improvement rate in figure 4. Specially, when the training data size is extremely small (smaller than 0.6), our model with only pre-training can achieve almost the same performance with ABD. This results may demonstrate the superiority of our model in small dataset, and our proposed pre-training strategy may alleviate the problem of the limited training sample in medical image analysis.

#### 5.4 Analysis of the hemispheric heterogeneity

In this subsection, we investigate the influence of heterogeneous graph on our model. Compared with the homogeneous graph based model, the main difference of our model is that we define two different connection modes. That is to say, the heterogeneous feature of our model is mainly reflected by the edge mapping function  $f_r(\cdot)$  ( $f_{intra}(\cdot)$  and  $f_{inter}(\cdot)$  in this work). Therefore, we intend to investigate the pattern of  $f_{intra}(\cdot)$  and  $f_{inter}(\cdot)$  in two graph modes (heterogeneous and homogeneous graph mode).

For homogeneous graph mode, inter- and intra-hemispheric edges are considered one type edge,

while the rest is still the same with heterogeneous mode. We define a Edge Mapping Scores as:

$$EMS_r = \frac{1}{T} \sum_T \frac{1}{|\mathcal{N}^r(t)|} \sum_{i,j} \text{Mean}(f_r(e_{ij})) \quad (11)$$

where  $T$  is the total number of subjects and  $\mathcal{N}^r(t)$  is the set of edge type  $r$  for subject  $t$ .  $EMS_r$  represents the activation of edge type  $r$  cross the subjects. We show the change of  $EMS_{Inter}$  and  $EMS_{Intra}$  during the training procedure. The result can be seen in figure 5.

We can see that, in heterogeneous graph mode, the  $EMS_{Inter}$  is lower than  $EMS_{Intra}$  at the beginning. With the increase of training epochs, the  $EMS_{Inter}$  increases faster than  $EMS_{Intra}$  and finally exceeded  $EMS_{Intra}$ . However, in homogeneous graph mode, the patterns of  $EMS_{Intra}$  and  $EMS_{Inter}$  have changed. The  $EMS_{Inter}$  is always less than  $EMS_{Intra}$  and the difference slightly increases during the training procedure.

From this phenomenon, we speculate that heterogeneous graph mode brings much more activation to inter-hemispheric edges. This mode assigns more importance to inter-hemispheric edges that may be neglected in homogeneous mode because of its low connection strength.

To demonstrate it, we conduct three extra experiments. We repeat disease prediction experiment in homogeneous graph model. Besides, we delete the intra-edges and inter-edges respectively to see the change of prediction performance. The result can be seen in table 3.

We can see that in homogeneous graph model, the prediction performance drops around 5%. More importantly, model that only contains inter-edges shows better performance than model that only contains intra-edges. This result may indicate that the inter-edges play an important role in brain network analysis.

## 5.5 Visualization

We visualize the embedding generate from proposed model to provide an intuitive evaluation. The results are shown in figure 6. We conduct the same readout strategy for initial FC and SC. Both SC and FC embedding are blurred cross subjects. After pre-training and finetuned with a MLP, the embeddings have a certain degree of distinction, while the boundary is still blurred. After supervised training, the embeddings show relatively clear boundary.

## 6 Future work

**More fine-grained modelling.** In this work, we introduce the concept of heterogeneous graph into brain network analysis. However, the modeling method in this work is still primary. It is necessary to model heterogeneous brain networks for specific diseases. For example, cognitive related diseases (e.g., Autistic Spectrum Disorder) may need construct node and edge types based on functional brain areas [57,58]. Diseases that have a significant impact on the physical structure of the brain (e.g., Parkinson’s Disease) may require building heterogenous brain network according to the relative position of nodes in the brain [59].

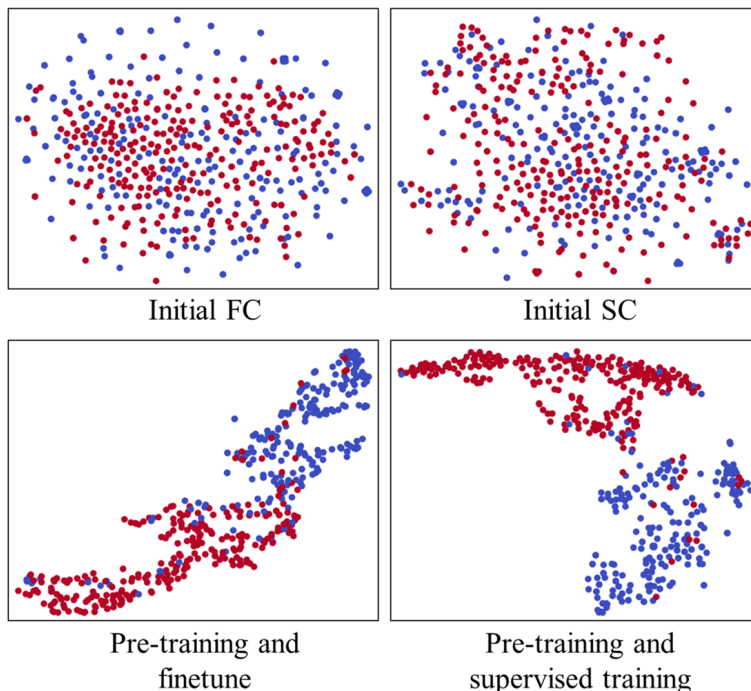


Figure 6: The t-SNE visualization of graph-level embeddings generated from model. The color of points represents the ground truth (the patient or health control).

**More powerful pre-training strategy.** Overfitting phenomenon usually occurs in medical image analysis fields, especially when the model becomes complicated. Traditional transfer learning method (supervised pre-training from another dataset) may not work well because of the limited labelled data. A more effective method is to pre-train the model in a self-supervised or unsupervised manner, which needs only unlabeled sample. Therefore, how to utilize the easy-accessible public datasets (e.g., PPMI [60], ABIDE [61,62], ADNI, HCP [63]) and pre-train the model more effectively is worth seriously considering.

**Brain temporal state analysis.** The human brain is a complicated dynamic system. Although there exist some literatures of dynamic-GNN models on neuroimaging data [64–66], there are few researches of the dynamic heterogeneous brain networks at date. Besides, the temporal resolution of fMRI data is not enough to explore the transient dynamic changes of the brain. Electroencephalogram (EEG) data with higher temporal resolution may be more suitable to characterize the dynamic state in the heterogeneous brain network, especially in the cognitive and emotional recognition tasks [67–69].

## 7 Conclusion

In this work, we propose a novel HGM model to encode the heterogeneous brain network. This model is inspired by the phenomenon of hemispheric lateralization and brain asymmetric. We creatively put forward that intra-hemispheric and inter-hemispheric edges have different patterns

and properties for brain network analysis. We apply our model to multimodal neuroimaging data (i.e., fMRI and DTI) fusion task and it shows great superiority compared with other methods. The analysis of the edge mapping scores (see section 5.4) shows that our model may attach more importance to inter-hemispheric edges and therefore achieve a better performance. Besides, we propose a novel self-supervised pre-training strategy designed for heterogeneous brain network, which is considered to alleviate the problem of limited training sample in medical image area. Finally, we propose several ideas to extend current model, including more fine-grained modelling methods, more powerful pre-train strategy and temporal state analysis in the brain.

## Acknowledgment

This research is supported in part by the National Natural Science Foundation of China (62071049, 61801026). Data used in the preparation of this article were obtained from the Alzheimer’s Disease Neuroimaging Initiative (ADNI) database ([adni.loni.usc.edu](http://adni.loni.usc.edu)). The ADNI was launched in 2003 as a public-private partnership, led by Principal Investigator Michael W. Weiner, MD. The primary goal of ADNI has been to test whether serial magnetic resonance imaging (MRI), positron emission tomography (PET), other biological markers, and clinical and neuropsychological assessment can be combined to measure the progression of mild cognitive impairment (MCI) and early Alzheimer’s disease (AD).

## References

- [1] M. W. Weiner *et al.*, “The alzheimer’s disease neuroimaging initiative 3: Continued innovation for clinical trial improvement,” *Alzheimer’s & Dementia*, 13(5):561–571, 2017.
- [2] C. P. Weingarten, M. H. Sundman, P. Hickey, and N. Chen, “Neuroimaging of parkinson’s disease: Expanding views,” *Neurosci. Biobehav. Rev.*, 59:16–52, 2015.
- [3] S. Klöppel, A. Abdulkadir, C. R. Jack Jr., N. Koutsouleris, J. Mourão-Miranda, and P. Vemuri, “Diagnostic neuroimaging across diseases,” *Neuroimage*, 61(2):457–463, 2012.
- [4] J. Fitzsimmons, M. Kubicki, and M. E. Shenton, “Review of functional and anatomical brain connectivity findings in schizophrenia,” *Curr. Opin. Psychiatry*, 26(2):172–87, 2013.
- [5] K. H. Karlsgodt, D. Sun, and T. D. Cannon, “Structural and functional brain abnormalities in schizophrenia,” *Curr. Dir. Psychol. Sci.*, 19(4):226–231, 2010.
- [6] D. Lei *et al.*, “Integrating machine learning and multimodal neuroimaging to detect schizophrenia at the level of the individual,” *Hum. Brain. Mapp.*, 41(5):1119–1135, 2020.
- [7] J. Sui *et al.*, “Combination of resting state fmri, dti, and smri data to discriminate schizophrenia by n-way mcca + jca,” *Front. Hum. Neurosci.*, 7(235), 2013.



- [8] M. E. Wagshul, M. Lucas, K. Ye, M. Izzetoglu, and R. Holtzer, “Multi-modal neuroimaging of dual-task walking: Structural mri and fnirs analysis reveals prefrontal grey matter volume moderation of brain activation in older adults,” *Neuroimage*, 189:745–754, 2019.
- [9] T. N. Kipf and M. Welling, “Semi-supervised classification with graph convolutional networks,” *arXiv preprint arXiv:1609.02907*, 2016.
- [10] H. Jiang, P. Cao, M. Xu, J. Yang, and O. Zaiane, “Hi-gcn: A hierarchical graph convolution network for graph embedding learning of brain network and brain disorders prediction,” *Comput. Biol. Med.*, 127:104096, 2020.
- [11] B. H. Kim and J. C. Ye, “Understanding graph isomorphism network for rs-fmri functional connectivity analysis,” *Front. Neurosci.*, 14(630), 2020.
- [12] X. Li, N. C. Dvornek, Y. Zhou, J. Zhuang, P. Ventola, and J. S. Duncan, “Graph neural network for interpreting task-fmri biomarkers,” In *MICCAI*, pages 485–493. Springer, 2019.
- [13] S. Parisot *et al.*, “Disease prediction using graph convolutional networks: Application to autism spectrum disorder and alzheimer’s disease,” *Med. Image. Anal.*, 48:117–130, 2018.
- [14] N. S. Dsouza, M. B. Nebel, D. Crocetti, J. Robinson, S. Mostofsky, and A. Venkataraman, “M-gcn: A multimodal graph convolutional network to integrate functional and structural connectomics data to predict multidimensional phenotypic characterizations,” In *MIDL*, 2021.
- [15] S. Wein *et al.*, “A graph neural network framework for causal inference in brain networks,” *Sc. Rep.*, 11(1):1–18, 2021.
- [16] D. Zhu *et al.*, “Fusing dti and fmri data: a survey of methods and applications,” *Neuroimage*, 102:184–91, 2014.
- [17] P. Bartolomeo and T. S. Malkinson, “Hemispheric lateralization of attention processes in the human brain,” *Curr. Opin. Psychol.*, 29:90–96, 2019.
- [18] K. Caeyenberghs and A. Leemans, “Hemispheric lateralization of topological organization in structural brain networks,” *Hum. Brain Mapp.*, 35(9):4944–4957, 2014.
- [19] A. W. Toga and P. M. Thompson, “Mapping brain asymmetry,” *Nat. Rev. Neurosci.*, 4(1):37–48, 2003.
- [20] G. Shi *et al.*, “The divided brain: Functional brain asymmetry underlying self-construal,” *NeuroImage*, 240:118382, 2021.
- [21] A. Brancucci, G. Lucci, A. Mazzatenta, and L. Tommasi, “Asymmetries of the human social brain in the visual, auditory and chemical modalities,” *Philos. Trans. R. Soc. Lond. B. Biol. Sci.*, 364(1519):895–914, 2009.
- [22] S. F. Carriba, Á. Loeches, A. Morcillo, and W. D. Hopkins, “Asymmetry in facial expression of emotions by chimpanzees,” *Neuropsychologia.*, 40(9):1523–1533, 2002.

- [23] A. Damasio, U. Bellugi, H. Damasio, H. Poizner, and J. Van Gilder, “Sign language aphasia during left-hemisphere amygdala injection,” *Nature*, 322(6077):363–5, 1986.
- [24] M. T. de Schotten *et al.*, “A lateralized brain network for visuospatial attention,” *Nat. Neurosci.*, 14(10):1245–1246, 2011.
- [25] J. J. Tanner *et al.*, “Marked brain asymmetry with intact cognitive functioning in idiopathic parkinson’s disease: a longitudinal analysis,” *Clin. Neuropsychol.*, 31(3):654–675, 2017.
- [26] N. J. Herzog and G. D. Magoulas, “Brain asymmetry detection and machine learning classification for diagnosis of early dementia,” *Sensors (Basel)*, 21(3), 2021.
- [27] P. Veličković, W. Fedus, W. L. Hamilton, P. Liò, Y. Bengio, and R. D. Hjelm, “Deep graph infomax,” *ICLR*, 2(3):4, 2019.
- [28] R. D. Hjelm *et al.*, “Learning deep representations by mutual information estimation and maximization,” *arXiv preprint arXiv:1808.06670*, 2018.
- [29] J. Yang, Q. Zhu, R. Zhang, J. Huang, D. Zhang, “Unified brain network with functional and structural data,” In *MICCAI*, pages 114–123. Springer, 2020.
- [30] A. Kumar, P. Rai, and H. Daume, “Co-regularized multi-view spectral clustering,” In *NeurIPS*, 24:1413–1421, 2011.
- [31] G. Ma, C. Lu, L. He, S. Philip, and A. B. Ragin, “Multi-view graph embedding with hub detection for brain network analysis,” In *ICDM*, pages 967–972. IEEE, 2017.
- [32] J. Li *et al.*, “Persistent feature analysis of multimodal brain networks using generalized fused lasso for emci identification,” In *MICCAI*, pages 44–52. Springer, 2020.
- [33] J. Huang, L. Zhou, L. Wang, and D. Zhang, “Attention-diffusion-bilinear neural network for brain network analysis,” *IEEE Trans. Med. Imaging.*, 39(7):2541–2552, 2020.
- [34] W. Zhang, L. Zhan, P. Thompson, and Y. Wang, “Deep representation learning for multimodal brain networks,” In *MICCAI*, pages 613–624. Springer, 2020.
- [35] A. Kazi *et al.*, “Inceptiongn: receptive field aware graph convolutional network for disease prediction,” In *IPMI*, pages 73–85. Springer.
- [36] S. Parisot *et al.*, “Disease prediction using graph convolutional networks: Application to autism spectrum disorder and alzheimer’s disease,” *Med. Image. Anal.*, 48:117–130, 2018.
- [37] X. Song *et al.*, “Graph convolution network with similarity awareness and adaptive calibration for disease-induced deterioration prediction,” *Med. Image. Anal.*, 69:101947, 2021.
- [38] B. Perozzi, R. Al-Rfou, and S. Skiena, “Deepwalk: Online learning of social representations,” In *SIGKDD*, pages 701–710, 2014.
- [39] P. Veličković *et al.*, “Graph attention networks,” *arXiv preprint arXiv:1710.10903*, 2017.

- [40] C. Shi, Y. Li, J. Zhang, Y. Sun, and P. S. Yu, “A survey of heterogeneous information network analysis,” *IEEE Trans. Knowl. Data. Eng.*, 29(1):17–37, 2016.
- [41] C. Yang, Y. Xiao, Y. Zhang, Y. Sun, and J. Han, “Heterogeneous network representation learning: A unified framework with survey and benchmark,” *IEEE Trans. Knowl. Data. Eng.*, 2020.
- [42] X. Wang *et al.*, “Heterogeneous graph attention network,” In *WWW*, pages 2022–2032, 2019.
- [43] Y. Dong, N. V. Chawla, and A. Swami, “metapath2vec: Scalable representation learning for heterogeneous networks,” In *SIGKDD*, pages 135–144, 2017.
- [44] M. Schlichtkrull, T. N. Kipf, P. Bloem, R. V. Den Berg, I. Titov, and M. Welling, “Modeling relational data with graph convolutional networks,” In *WSWC*, pages 593–607. Springer, 2018.
- [45] C. Zhang, D. Song, C. Huang, A. Swami, and N. V. Chawla, “Heterogeneous graph neural network,” In *SIGKDD*, pages 793–803, 2019.
- [46] T. Mikolov, I. Sutskever, K. Chen, G. S. Corrado, and J. Dean, “Distributed representations of words and phrases and their compositionality,” In *NeurIPS*, pages 3111–3119, 2013.
- [47] J. M. Giorgi, O. Nitski, G. D. Bader, and B. Wang, “Declutr: Deep contrastive learning for unsupervised textual representations,” *arXiv preprint arXiv:2006.03659*, 2020.
- [48] T. Chen, S. Kornblith, M. Norouzi, and G. Hinton, “A simple framework for contrastive learning of visual representations,” In *ICML*, pages 1597–1607, 2020. PMLR.
- [49] X. Chen, H. Fan, R. Girshick, and K. He, “Improved baselines with momentum contrastive learning,” *arXiv preprint arXiv:2003.04297*, 2020.
- [50] J. Qiu *et al.*, “Gcc: Graph contrastive coding for graph neural network pre-training,” In *SIGKDD*, pages 1150–1160, 2020.
- [51] Y. You, T. Chen, Y. Sui, T. Chen, Z. Wang, and Y. Shen, “Graph contrastive learning with augmentations,” In *NeurIPS*, 33:5812–5823, 2020.
- [52] M. D. Donsker and S. R. S. Varadhan, “Asymptotic evaluation of certain markov process expectations for large time, I,” *Commun. Pure. Appl. Math.*, 28(1):1–47, 1975.
- [53] S. Nowozin, B. Cseke, and R. Tomioka, “f-gan: Training generative neural samplers using variational divergence minimization,” In *NeurIPS*, pages 271–279, 2016.
- [54] J. Wang, X. Wang, M. Xia, X. Liao, A. Evans, and Y. He, “Gretna: a graph theoretical network analysis toolbox for imaging connectomics,” *Front. Hum. Neurosci.*, 9(386), 2015.
- [55] L. Fan *et al.*, “The human brainnetome atlas: A new brain atlas based on connectional architecture,” *Cereb Cortex*, 26(8):3508–26, 2016.

- [56] F. C. Yeh, T. D. Verstynen, Y. Wang, J. C. Fernández-Miranda, and W. Y. I. Tseng, “Deterministic diffusion fiber tracking improved by quantitative anisotropy,” *PLoS ONE*, 8(11):e80713, 2013.
- [57] E. Hill, S. Berthoz, and U. Frith, “Brief report: Cognitive processing of own emotions in individuals with autistic spectrum disorder and in their relatives,” *J. Autism. Dev. Disord.*, 34(2):229–235, 2004.
- [58] L. Q. Uddin, B. T. Thomas Yeo, and R. N. Spreng, “Towards a universal taxonomy of macro-scale functional human brain networks,” *Brain. Topogr.*, 32(6):926–942, 2019.
- [59] S. I. Ktena *et al.*, “Metric learning with spectral graph convolutions on brain connectivity networks,” *NeuroImage*, 169:431–442, 2018.
- [60] K. Marek *et al.*, “The parkinson progression marker initiative (ppmi),” *Prog. Neurobiol.*, 95(4):629–635, 2011.
- [61] A. D. Martino *et al.*, “The autism brain imaging data exchange: towards a large-scale evaluation of the intrinsic brain architecture in autism,” *Mol. Psychiatry.*, 19(6):659–667, 2014.
- [62] A. D. Martino *et al.*, “Enhancing studies of the connectome in autism using the autism brain imaging data exchange ii,” *Sci. Data.*, 4(1):170010, 2017.
- [63] D. C. V. Essen *et al.*, “The wu-minn human connectome project: an overview,” *Neuroimage*, 80:62–79, 2013.
- [64] D. Yao, J. Sui, E. Yang, P. Yap, D. Shen, and M. Liu, “Temporal-adaptive graph convolutional network for automated identification of major depressive disorder using resting-state fmri,” In *MLMI workshop*, pages 1–10, 2020. Springer.
- [65] X. Xing *et al.*, “Dynamic spectral graph convolution networks with assistant task training for early mci diagnosis,” In *MICCAI*, pages 639–646, 2019. Springer.
- [66] S. Gadgil, Q. Zhao, A. Pfefferbaum, E. V. Sullivan, E. Adeli, and K. M. Pohl, “Spatio-temporal graph convolution for resting-state fmri analysis,” In *MICCAI*, pages 528–538, 2020. Springer.
- [67] O. Bazgir, Z. Mohammadi, and S. A. H. Habibi, “Emotion recognition with machine learning using eeg signals,” In *ICBME*, pages 1–5, 2018. IEEE.
- [68] M. Kim, M. Kim, E. Oh, and S. Kim, “A review on the computational methods for emotional state estimation from the human eeg,” *Comput. Math. Methods. Med.*, vol. 2013, 2013.
- [69] H. Bo, L. Ma, Q. Liu, R. Xu, and H. Li, “Music-evoked emotion recognition based on cognitive principles inspired eeg temporal and spectral features,” *Int. J. Mach. Learn. Cybern.*, 10(9):2439–2448, 2019.
- [70] Zhang, Y., Zhan, L., Cai, W., Thompson, P., and Huang, H, “Integrating heterogeneous brain networks for predicting brain disease conditions,” In *MICCAI*, pages 214–222, 2019. Springer.

- [71] Gürbüz, M. B., and Rekik, I, “MGN-Net: A multi-view graph normalizer for integrating heterogeneous biological network populations,” *Med. Image. Anal.*, 71, 102059, 2021
- [72] Wang, *Jet al.*, “Functional network estimation using multigraph learning with application to brain maturation study,” *Hum. Brain. Mapp.*, 42(9), 2880-2892, 2021
- [73] Wang, Xiao, et al., “Self-supervised Heterogeneous Graph Neural Network with Co-contrastive Learning,” *arXiv preprint arXiv:2105.09111*, 2021.

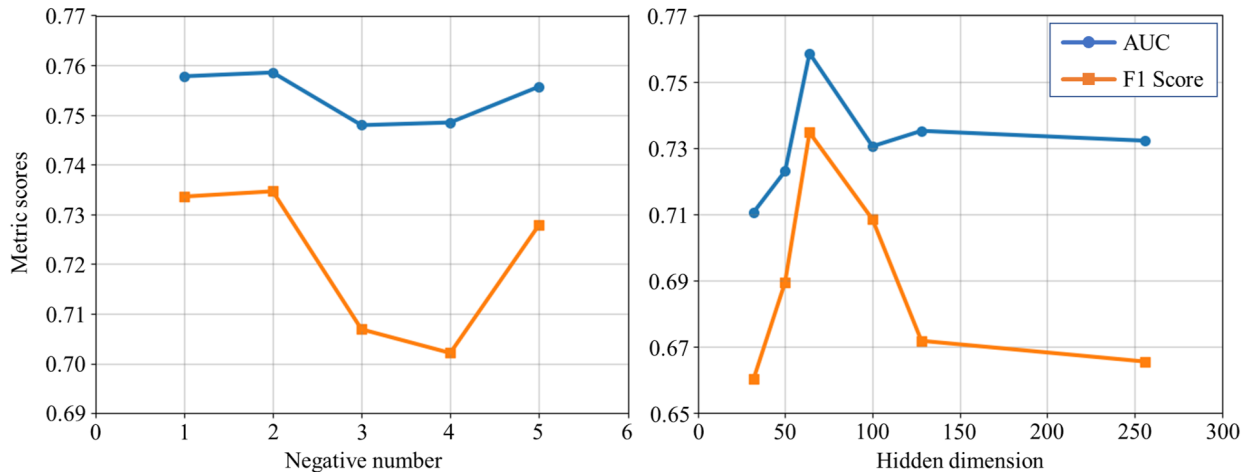


Figure 7: The sensitivity of two main hyper-parameters (The number of negative sampling and Node hidden dimension).

## A Appendix

### A.1 Implementation details

For OH dataset, the model contains 1 hidden layer and the hidden dimension is 64. Batch size is 128 and dropout is 0.75. The learning rate is  $1e-4$  and L2 regularization is  $1e-5$ . The MLP for prediction contains 1 linear layer. The model is pre-trained 10 epochs with  $K = 1$  and then supervised training 40 epochs (totally 50 epochs).

For ADNI dataset, the model architecture is the same. Hidden dimension is still 64. Batch size is 128 and dropout is 0.7. The learning rate is  $1e-4$  and  $2.5e-4$  for pre-training and supervised training, respectively. L2 regularization is  $1e-5$ . The model is pre-trained 20 epochs with  $K = 2$  and then supervised training 175 epochs (totally 195 epochs).

For baseline models, the architecture is the default and hidden dimension is also 64. The number of heads for GAT is 4. The hyperparameters  $(D, K_1, K_2)$  for MGCN model are set to  $D = 256$ ,  $K_1 = 128$ ,  $K_2 = 64$ . For DMBN model, the numbers of positive layer and negative layer are 1 in ADNI dataset and the number of head is 2. The numbers of positive layer and negative layer are 5 and 4 respectively in OH dataset and the number of head is 4.

### A.2 Parameter sensitivity analysis

In this subsection, we investigate the sensitivity of the two main hyper-parameters, including the number of negative sampling and node hidden dimensions. The results are shown in figure 7.

We can see that the number of negative sampling has a small impact on the model performance. We think a small value of  $K$  may be enough for the dataset. However, compared with negative sampling number, the node hidden dimension has a relative greater impact on model performance. With the increase of node hidden dimension, the performance get a rise first and then declines. This result may show that a suitable hidden dimension is needed for the model.